

Fonseca Teixeira, L.M., et al., 2023, The dynamic nature of  $a\text{TiO}_2$ : Implications for Ti-based thermometers in magmatic systems: *Geology*, <https://doi.org/10.1130/G51587.1>

## Supplemental Material

**Fitting and calculation procedures and published data sets utilized in this study shown in supplemental data files 1 and 2.**

## SUPPLEMENTARY DATA 1

### 1. Modelling $a\text{TiO}_2$ in natural systems

Source data for titanium activities ( $a\text{TiO}_2$ ) at different magmatic temperatures from Ghiorso and Gualda (2013) are available in Supplementary data 2. In the following, we briefly describe how we derive the equation for fitting  $a\text{TiO}_2$  as a function of temperature for the examples shown in Fig. 1 in the main text.

Based on the solubility model of Borisov and Aranovich (2020), the activity of  $\text{TiO}_2$  in a melt relative to rutile saturation can be expressed with:

$$a\text{TiO}_2^{\text{liq-rutile}} = \frac{a\text{TiO}_2^{\text{melt}}}{a\text{TiO}_2^{\text{melt saturated}}} \quad (\text{Eqn S1})$$

Whereby  $a\text{TiO}_2^{\text{liq-rutile}} = 1$  when the melt is rutile-saturated. Based on the solubility model of Borisov and Aranovich (2020),  $a\text{TiO}_2$  can be expressed with:

$$a\text{TiO}_2^{\text{liq-rutile}} = \gamma\text{TiO}_2^{\text{liq-rutile}} \cdot X_{\text{TiO}_2} \quad (\text{Eqn S2})$$

Here,  $X_{\text{TiO}_2}$  is the mole fraction of  $\text{TiO}_2$  in the melt and  $\gamma\text{TiO}_2^{\text{liq-rutile}}$  is the  $\text{TiO}_2$  activity coefficient. Based on the rutile solubility model of Borisov and Aranovich (2020, their Eqn. 8),  $\gamma\text{TiO}_2^{\text{liq-rutile}}$  can be expressed as

$$-\log \gamma\text{TiO}_2^{\text{liq-rutile}} = (2228 X_{\text{SiO}_2}^2 - 8419 X_{\text{SiO}_2} \cdot X_{\text{Al}_2\text{O}_3} - 5028 X_{\text{SiO}_2} \cdot X_{\text{FeO}} - 6151 X_{\text{SiO}_2} \cdot X_{\text{Na}_2\text{O}} + 24821 X_{\text{Al}_2\text{O}_3} \cdot X_{\text{K}_2\text{O}} + 77332 X_{\text{FeO}} \cdot X_{\text{Na}_2\text{O}} - 15552 X_{\text{MgO}} \cdot X_{\text{CaO}} + 29030 X_{\text{CaO}} \cdot X_{\text{Na}_2\text{O}} - 1207)/(T+273.15) - 0.0112 P + 0.66 \quad (\text{Eqn S3})$$

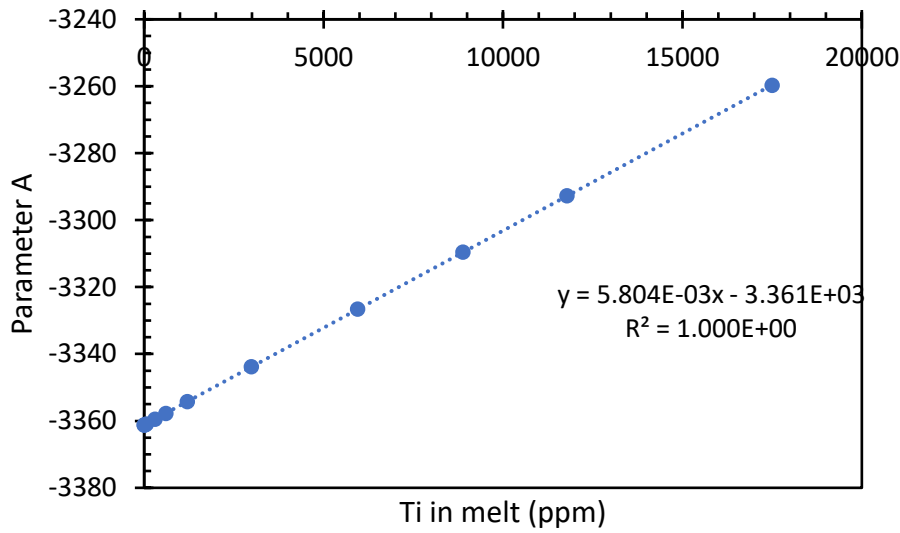
Where  $X_{\text{oxide}}$  are the respective oxide mole fractions of in a melt,  $T$  is temperature in  $^\circ\text{C}$  and  $P$  is pressure in kbar. At a pressure of 2 kbar, representative of a shallow silicic magmatic system, we can shorten this equation to

$$-\log \gamma\text{TiO}_2^{\text{liq-rutile}} = A/(T+273.15) + 0.638 \quad (\text{Eqn S4})$$

where  $A$  summarizes all terms contained in the first bracket in Eqn. S3 and exclusively depends on the composition of the melt.

Assuming that the composition remains roughly constant and only the Ti content varies in the melt (as likely appropriate for these high-silica rhyolites close to a minimum composition), mole fractions of all other elements will vary as a function of  $X_{\text{TiO}_2}$  due to the continuous relative dilution of other oxides with increasing  $\text{TiO}_2$  contents, thus controlling parameter A. For an average Yellowstone rhyolite composition, we can parameterize the relationship between the Ti content in the melt (in ppm, normalized anhydrous) and parameter A, finding that

$$A = 5.798 \cdot 10^{-3} \cdot \text{Ti}_{\text{melt}} - 3361 \quad (\text{Eqn S5})$$



Simultaneously,  $X_{\text{TiO}_2}$  can also be expressed through the Ti content in the melt (in ppm, normalized anhydrous) with

$$X_{\text{TiO}_2} = 1.360 \cdot 10^{-6} \cdot \text{Ti}_{\text{melt}} - 6.416 \cdot 10^{-6} \quad (\text{Eqn S6})$$

Substituting Eqns. S4, S5, and S6 into Eqn. S3, we can express the Ti activity in a melt of constant major element composition relative to rutile saturation with

$$a_{\text{TiO}_2}^{\text{liq-rutile}} = 10^{-(5.798 \cdot 10^{-3} \cdot \text{Ti}_{\text{melt}} - 3361)/(T+273.15) + 0.638} \cdot (1.360 \cdot 10^{-6} \cdot \text{Ti}_{\text{melt}} - 6.416 \cdot 10^{-6}) \quad (\text{Eqn S7})$$

To calculate a typical evolution of Ti activities with temperature, we consider as a first approximation that the Ti content in the melt varies linearly as a function of temperature  $T$  (in  $^{\circ}\text{C}$ )

$$Ti_{melt}(T) = \frac{\partial Ti}{\partial T} T + B \quad (\text{Eqn S8})$$

where B is the intercept at  $T = 0$  °C. For a given system, parameter B can be expressed as a function of the melt Ti content at a given magmatic temperature ( $T_a$ ), for example immediately prior to eruption so that B can be constrained from the estimated pre-eruptive temperature of a system and the melt Ti contents as measured in volcanic glass

$$B = Ti_{melt}(T_a) - \frac{\partial Ti}{\partial T} T_a \quad (\text{Eqn S9})$$

By substituting S8 and S9 into Eqn. S7, we obtain an expression for the Ti activity in a system undergoing a linear change in melt Ti contents with temperature:

$$a_{TiO_2}^{liq-rutile} = 10^{-(5.798 \cdot 10^{-3} \cdot \frac{\partial Ti}{\partial T} T + Ti_{melt}(T_a) - \frac{\partial Ti}{\partial T} T_a - 3361)/(T+273.15) + 0.638) \cdot (1.360 \cdot 10^{-6} \cdot \frac{\partial Ti}{\partial T} T + Ti_{melt}(T_a) - \frac{\partial Ti}{\partial T} T_a - 6.416 \cdot 10^{-6}) \quad (\text{Eqn S10})$$

As a last step, we account for a variable rate of Ti removal or increase in the melt as the amount of crystallization of Ti-rich phases is likely to vary with temperature and Ti content in the melt. We can approximate this behaviour by letting  $\partial Ti / \partial T$  vary linearly with T:

$$\frac{\partial Ti}{\partial T}(T) = \frac{\partial^2 Ti}{\partial T^2} \cdot T + \left( \frac{\partial Ti}{\partial T} \right)_{T=0} \quad (\text{Eqn S11})$$

Substituting Eqn S11 into S10 results in the final equation that we use for the fitting procedure:

$$a_{TiO_2}^{liq-rutile} = 10^{-(5.798 \cdot 10^{-3} \cdot \left( \frac{\partial^2 Ti}{\partial T^2} \cdot T + \left( \frac{\partial Ti}{\partial T} \right)_{T=0} \right) T + Ti_{melt}(T_a) - \left( \frac{\partial^2 Ti}{\partial T^2} \cdot T + \left( \frac{\partial Ti}{\partial T} \right)_{T=0} \right) T_a - 3361)/(T+273.15) + 0.638) \cdot (1.360 \cdot 10^{-6} \cdot \left( \frac{\partial^2 Ti}{\partial T^2} \cdot T + \left( \frac{\partial Ti}{\partial T} \right)_{T=0} \right) T + Ti_{melt}(T_a) - \left( \frac{\partial^2 Ti}{\partial T^2} \cdot T + \left( \frac{\partial Ti}{\partial T} \right)_{T=0} \right) T_a - 6.416 \cdot 10^{-6}) \quad (\text{Eqn S12})$$

We use this equation to fit  $a_{TiO_2}^{liq-rutile}$  values at different magmatic temperatures from the dataset in Ghiorso and Gualda (2013) for Bishop Tuff, Fish Canyon Tuff, Yellowstone and Shiveluch volcanic centers. During the fitting procedure, the parameters  $T_a$ ,  $Ti_{melt}(T_a)$ ,  $\left( \frac{\partial Ti}{\partial T} \right)_{T=0}$ , and  $\frac{\partial^2 Ti}{\partial T^2}$  were not bounded, and best-fit values were calculated by the curving fitting

tool in Matlab. Below, we report all coefficients and information on the goodness of fit for the four examples (Table S1) and chosen compositions for each example (Table S2). Starting estimates for best-fits of  $T_a$  were chosen corresponding to the highest temperature at which oxides precipitate.

For the curves displayed in Fig. 1 in the main text, we assume that no  $\text{TiO}_2$  removal occurred prior to Fe-Ti oxide precipitation and begin the calculation of  $a\text{TiO}_2^{\text{liq-rutile}}$  through Eqn. S8 at the highest recorded Fe-Ti temperature estimate (except for Shiveluch, as noted before). At higher temperatures prior to Fe-Ti oxide saturation,  $a\text{TiO}_2^{\text{liq-rutile}}$  follows the solubility curves shown in grey in Fig. 1 in the main text.

Table S1: Best-fit parameters for modelling  $a\text{TiO}_2$  in natural systems

Bishop Tuff	Fish Canyon Tuff
<b>General model:</b>	<b>General model:</b>
$f(x) = (10^{-(6.043\text{E-}03*((B*x+C)*x+A-(B*x+C)*T)-3458)/(x+273.15)+0.638))$ $*(1.356\text{E-}6 * ((B*x+C)*x+A-(B*x+C)*T)-6.9496\text{E-}6)$	$f(x) = (10^{-(5.481\text{E-}03*((B*x+C)*x+A-(B*x+C)*T)-3245)/(x+273.15)+0.638))$ $*(1.359\text{E-}6*((B*x+C)*x+A-(B*x+C)*T)-6.398\text{E-}6)$
<b>Coefficients (with 95% confidence bounds):</b>	<b>Coefficients (with 95% confidence bounds):</b>
$A = \text{TiO}_2^{\text{melt}}(T_a) = 1724 \text{ } (-1.471\text{e}+08, 1.471\text{e}+08)$	$A = \text{TiO}_2^{\text{melt}}(T_a) = 1704 \text{ } (-8.048\text{e}+08, 8.048\text{e}+08)$
$B = \partial^2\text{TiO}_2/\partial T^2 = 0.02261 \text{ } (0.0214, 0.02382)$	$B = \partial^2\text{TiO}_2/\partial T^2 = 0.006754 \text{ } (-0.03081, 0.04432)$
$C = \partial\text{TiO}_2/\partial T(T=0) = -6.822 \text{ } (-2.71\text{e}+05, 2.71\text{e}+05)$	$C = \partial\text{TiO}_2/\partial T(T=0) = 3.225 \text{ } (-6.514\text{e}+05, 6.514\text{e}+05)$
$T = T_a = 844.4 \text{ } (-1.199\text{e}+07, 1.199\text{e}+07)$	$T = T_a = 758 \text{ } (-9.644\text{e}+07, 9.644\text{e}+07)$
<b>Goodness of fit:</b>	<b>Goodness of fit:</b>
<b>SSE: 0.04025</b>	SSE: 0.02205
R-square: 0.9229	R-square: 0.6239
Adjusted R-square: 0.9204	Adjusted R-square: 0.5371
RMSE: 0.0208	RMSE: 0.04119

Yellowstone	Shiveluch
<b>General model:</b>	<b>General model:</b>
$f(x) = (10^{-(5.798E-03*((B*x+C)*x+A-(B*x+C)*T)-3361)/(x+273.15)+0.638))$ $*(1.36E-6*((B*x+C)*x+A-(B*x+C)*T)-6.416E-6)$	$f(x) = (10^{-(6.019E-03*((B*x+C)*x+A-(B*x+C)*T)-3463)/(x+273.15)+0.638))$ $*(1.348E-6*((B*x+C)*x+A-(B*x+C)*T)-6.953E-6)$
<b>Coefficients (with 95% confidence bounds):</b>	<b>Coefficients (with 95% confidence bounds):</b>
$A = TiO_2^{melt}(T_a) = 3083 \text{ } (-1.041e+09, 1.041e+09)$ $B = \partial^2 TiO_2 / \partial T^2 = 0.03611 \text{ } (0.02303, 0.04919)$ $C = \partial TiO_2 / \partial T(T=0) = -14.24 \text{ } (-1.882e+06, 1.882e+06)$ $T = T_a = 947.3 \text{ } (-5.211e+07, 5.211e+07)$	$A = TiO_2^{melt}(T_a) = 2604 \text{ } (-5.097e+08, 5.097e+08)$ $B = \partial^2 TiO_2 / \partial T^2 = 0.0203 \text{ } (0.01484, 0.02577)$ $C = \partial TiO_2 / \partial T(T=0) = -5.553 \text{ } (-8.132e+05, 8.132e+05)$ $T = T_a = 900.2 \text{ } (-4.005e+07, 4.005e+07)$
<b>Goodness of fit:</b>	<b>Goodness of fit:</b>
SSE: 0.02108	SSE: 0.008577
R-square: 0.7543	R-square: 0.9296
Adjusted R-square: 0.7223	Adjusted R-square: 0.9199
RMSE: 0.03028	RMSE: 0.01975

Table S2: Compositions used to model aTiO<sub>2</sub> in natural systems. Compositions exclude TiO<sub>2</sub> and are not normalised (normalisation occurs during fitting procedure). Yellowstone-Heise averaged composition from Troch et al. (2020); Fish Canyon Tuff the full deposition sequence averaged from Whitney and Stormer (1985); Shiveluch 2001-2004 eruptions averaged from Blundy et al. (2006); Bishop Tuff fall layers and early ignimbrites (early-erupted Bishop Tuff) averaged from Chamberlain et al. (2015).

	Yellowstone	Bishop Tuff	Fish Canyon	Shiveluch
<b>SiO<sub>2</sub></b>	75.15	74.55	74.00	74.58
<b>Al<sub>2</sub>O<sub>3</sub></b>	12.26	12.24	12.22	12.43
<b>FeO<sub>tot</sub></b>	3.43	0.65	3.04	1.20
<b>MgO</b>	0.13	0.05	0.61	0.27
<b>CaO</b>	0.62	0.50	1.66	0.94
<b>Na<sub>2</sub>O</b>	3.27	3.52	2.55	4.57

<b>K<sub>2</sub>O</b>	4.86	4.64	5.89	3.10
-----------------------	------	------	------	------

---

## 2. Calculating Ti-in-quartz for fixed and dynamic $a_{\text{TiO}_2}$ in the same system

Using the activities and temperatures from Ghiorso and Gualda (2013), available in Supplementary data 2, the Ti-in-quartz calibration of Huang and Audétat (2012), for a fixed pressure of 2 kbar (based on the Bishop Tuff system), we calculated how much Ti would be found in quartz crystals, if quartz co-crystallized with Fe-oxides (Panel B, Fig. 4).

Using the Ti in quartz (ppm) from Panel B, we calculate crystallization temperatures assuming a fixed  $a_{\text{TiO}_2}^{\text{liq-rutile}} = 0.5$  (Panel C, Fig. 4). Temperatures from Panel C were subtracted from temperatures from Panel B, resulting in the offset observed in Panel D (Fig. 4).

## 3. Mixing Bishop Tuff compositions

For a pre-mixing Bishop Tuff composition, we chose the early-erupted Bishop Tuff's most SiO<sub>2</sub>-rich glass composition from the first erupted Fall layer (F1) from the dataset from Chamberlain et al. (2015), reported below. We added H<sub>2</sub>O and CO<sub>2</sub> content from early-erupted Bishop Tuff (EBT) melt inclusions reported by Wallace et al. (1999).

For the recharged melt, we used a Mono Lake andesite from the Long Valley (Bailey, 1962). For CO<sub>2</sub>, we used the highest observed CO<sub>2</sub> content in the late-erupted Bishop Tuff (~1000 ppm), as this is higher than numbers usually reported for basalts (Wallace et al., 1999). For H<sub>2</sub>O content, we used 4% as it is also reported for the late-erupted Bishop Tuff by Wallace et al. (1999).

Compositions were normalised to 100 wt% anhydrous. Dacite mass fractions of 5%, 7%, and 13% were used for the mixing. For comparison, we provide a few late-erupted Bishop Tuff glass analyses from Chamberlain et al. (2015) – these do not include H<sub>2</sub>O and CO<sub>2</sub> contents, and hence are not normalised, but the addition of these oxides would not change the compositions significantly.

Melt Ti activities  $a_{\text{TiO}_2}^{\text{liq-rutile}}$  are calculated for potential post mixing temperatures from 900 to 700 °C, with 50 °C intervals, using the model of Borisov and Aranovich (2020).

Table S3: Early-erupted Bishop Tuff (EBT) F1 composition before mixing (Chamberlain et al., 2015), Mono Lake andesite from the Long Valley (Bailey, 1962), and mixed compositions at different basalt fractions (5, 7, 13%)

	EBT before mixing		Long Valley andesite		After mixing		
	EBT F1	norm	andesite	norm	5%	7%	13%
<b>SiO<sub>2</sub></b>	76.02	74.02	62.90	64.62	73.55	73.36	72.80
<b>Al<sub>2</sub>O<sub>3</sub></b>	12.04	11.72	16.60	17.05	11.99	12.10	12.42
<b>TiO<sub>2</sub></b>	0.07	0.07	1.01	1.04	0.12	0.14	0.19
<b>FeO</b>	0.67	0.65	4.03	4.14	0.83	0.90	1.11
<b>MgO</b>	0.01	0.01	1.23	1.26	0.07	0.10	0.17
<b>CaO</b>	0.42	0.41	3.27	3.36	0.56	0.62	0.79
<b>Na<sub>2</sub>O</b>	3.37	3.28	4.49	4.61	3.35	3.37	3.45
<b>K<sub>2</sub>O</b>	4.80	4.67	3.52	3.62	4.62	4.60	4.54
<b>H<sub>2</sub>O</b>	5.30	5.16	0.28	0.29	4.92	4.82	4.53
<b>CO<sub>2</sub></b>	0.01	0.01	0.01	0.01	0.01	0.01	0.01
<b>Total</b>	102.71	100.00	103.13	100.00	100.00	100.00	100.00

Table S4: Example analyses in late-erupted Bishop Tuff glass (Chamberlain et al., 2015)

<b>Sample</b>	BP218	BP211	BP198	BP198	BP015	BP004
<b>Unit</b>	Ig2NWb	Ig2NWb	Ig2Ea	Ig2Ea	Ig2Nb	Ig2Ea
<b>Shard tag</b>	G13_1	G3_4	G1_2	G14_1	G8_2	G12_1
<b>SiO<sub>2</sub></b>	68.47	69.53	68.90	68.47	72.90	72.38
<b>Al<sub>2</sub>O<sub>3</sub></b>	13.48	15.61	14.98	14.29	11.80	11.84
<b>TiO<sub>2</sub></b>	0.21	0.71	0.20	0.26	0.15	0.07
<b>FeO</b>	1.10	1.89	2.38	2.75	0.67	0.70
<b>MgO</b>	0.03	1.37	1.02	1.06	0.09	0.04
<b>CaO</b>	1.53	1.89	2.25	2.10	0.53	0.42
<b>Na<sub>2</sub>O</b>	2.29	3.38	3.94	3.84	3.09	3.34
<b>K<sub>2</sub>O</b>	5.14	4.94	4.29	4.53	4.80	4.57



Table S5:  $a_{\text{TiO}_2}$  for different andesite fractions and various temperatures after mixing.

**$a_{\text{TiO}_2}$  for compositions after mixing**

Andesite						
fraction	TiO <sub>2</sub> in melt	T = 900°C	T = 850°C	T = 800°C	T = 750°C	T = 700°C
5%	0.12	0.20	0.27	0.38	0.54	0.81
7%	0.14	0.23	0.31	0.43	0.62	0.92
13%	0.19	0.3	0.41	0.56	0.8	1.19*

Activities in red (\*) represent TiO<sub>2</sub>-saturation conditions and should be considered as 1.0.

#### 4. Conversion of Ti to TiO<sub>2</sub>

In whole rock compositions and minerals, titanium is often measured as pure Ti, instead of its oxide form (TiO<sub>2</sub>). However, as TiO<sub>2</sub> solubility and activity are given in relation to the oxide, we provide the following conversion factor:

**1 ppm of Ti = 0.6 ppm of TiO<sub>2</sub>**

Or

**TiO<sub>2</sub> = Ti/0.6**

## SUPPLEMENTARY DATA 2

Table S6:  $a_{\text{TiO}_2}$  from Fe-Ti oxides, retrieved from Ghiorso and Gualda (2013).

## References

- Bailey, R.A., 1962, Eruptive History and Chemical Evolution of the Precaldera and Postcaldera Basalt-dacite Sequences, Long Valley, California: Implications for Magma Sources, Current Seismic Unrest, and Future Volcanism: U.S. Department of the Interior, U.S. Geological Survey, 88 p.
- Blundy, J., Cashman, K., and Humphreys, M., 2006, Magma heating by decompression-driven crystallization beneath andesite volcanoes: Nature, v. 443, p. 76–80, doi:10.1038/nature05100.

- Borisov, A., and Aranovich, L., 2020, Rutile solubility and TiO<sub>2</sub> activity in silicate melts: An experimental study: *Chemical Geology*, v. 556, p. 119817, doi:10.1016/j.chemgeo.2020.119817.
- Chamberlain, K.J., Wilson, C.J.N., Wallace, P.J., and Millet, M.-A., 2015, Micro-analytical Perspectives on the Bishop Tuff and its Magma Chamber: *Journal of Petrology*, v. 56, p. 605–640, doi:10.1093/petrology/egv012.
- Ghiorso, M.S., and Gualda, G.A.R., 2013, A method for estimating the activity of titania in magmatic liquids from the compositions of coexisting rhombohedral and cubic iron–titanium oxides: *Contributions to Mineralogy and Petrology*, v. 165, p. 73–81, doi:10.1007/s00410-012-0792-y.
- Huang, R., and Audétat, A., 2012, The titanium-in-quartz (TitaniQ) thermobarometer: A critical examination and re-calibration: *Geochimica et Cosmochimica Acta*, v. 84, p. 75–89, doi:10.1016/j.gca.2012.01.009.
- Troch, J., Ellis, B.S., Harris, C., Bachmann, O., and Bindeman, I.N., 2020, Low- $\delta^{18}\text{O}$  silicic magmas on Earth: A review: *Earth-Science Reviews*, v. 208, p. 103299, doi:10.1016/j.earscirev.2020.103299.
- Wallace, P.J., Anderson Jr., A.T., and Davis, A.M., 1999, Gradients in H<sub>2</sub>O, CO<sub>2</sub>, and exsolved gas in a large-volume silicic magma system: Interpreting the record preserved in melt inclusions from the Bishop Tuff: *Journal of Geophysical Research: Solid Earth*, v. 104, p. 20097–20122, doi:10.1029/1999JB900207.
- Whitney, J.A., and Stormer, J.C., JR., 1985, Mineralogy, Petrology, and Magmatic Conditions from the Fish Canyon Tuff, Central San Juan Volcanic Field, Colorado: *Journal of Petrology*, v. 26, p. 726–762, doi:10.1093/petrology/26.3.726.